Available online at https://link.springer.com/journal/42241
http://www.jhydrodynamics.com
Journal of Hydrodynamics, 2021
https://doi.org/10.1007/s42241-021-0046-4

Liutex-based centripetal force field model for improving the resistance and wake performances of JBC ship sailing in calm water *

Xin-wang Liu[1], Song-tao Chen[1], Wei-wen Zhao[1], De-cheng Wan[1, 2], Yi-qian Wang[3]
1. *Computational Marine Hydrodynamics Lab (CMHL), School of Naval Architecture, Ocean and Civil Engineering, Shanghai Jiao Tong University, Shanghai 200240, China*
2. *Ocean College, Zhejiang University, Zhoushan 316021, China*
3. *School of Mathematical Science, Soochow University, Suzhou 215006, China*

(Received May 7, 2021, Revised June 8, 2021, Accepted June 9, 2021, Published online June 28, 2021)

Abstract: For complex aerodynamic and hydrodynamic problems, the analysis of vortex is very important. The Liutex method is an eigenvalue-based method which is local, accurate, and unique, which can give an accurate definition of vortex, so the control of vortex can be implemented and effectively guaranteed. Based on Liutex method, two methodologies of centripetal force model and counter-rotation force model were proposed to illustrate the vortex dynamics and possibly strengthen or weaken the vortices. In this paper, the Liutex-based centripetal force model is applied by adding a source term to the Navier-Stokes equations. In order to investigate the influence of the constructed Liutex force model on the 3-dimensional flow around a slow-fat ship, the calm-water drag calculation result of JBC ship is regarded as the initial flow field, and the new resistance and wake performances of the ship are obtained after applying the centripetal force model to the flow field with different strengths. Several views of the comparisons of the new steady flow fields are shown, and the parametric study results indicate that the Liutex-based centripetal force model can effectively change the resistance and wake performances of the JBC ship, which provides a new idea and theoretical basis for the comprehensive hydrodynamic performance optimization of the ship hull.

Key words: Vortex dynamics, Liutex vector, flow control, ship resistance, ship wake, ship hydrodynamic optimization

Introduction

For complex aerodynamic and hydrodynamic problems, the analysis of vortex is very important, because it vividly represents the rotation effect of velocity field, and has a direct impact on the performance of aircraft and marine structures. In order to achieve the purpose of flow field control, existing researches generally focus on adding some small structures similar to appendage to the original structure, or directly change the shape or layout of the structure, so as to achieve the optimization of aero- or hydro-dynamic performances, that is, by changing the boundary shape of the flow field to achieve flow field control. From another point of view, we can also directly change the flow field numerically. On the one hand, it can be cheaper to implement and convenient to analyse the mechanism of flow field change, on the other hand, it may provide a new idea for the optimization design of actual structures such as aircraft and ships.

In order to control vortices directly, an accurate definition of vortex should be obtained. According to Liu et al.[1], the vortex identification (VI) methods can be divided into three generations. The first-generation VI methods are based on vorticity, which are not sufficient to represent the vortical structures because of the weak correlation between vorticity and vortex, especially in the near wall region for the wall-bounded flows. The second-generation VI methods were then proposed to tackle this problem. Typical examples include Q, λ_2, Δ, λ_{ci} and other methods[2-5]. However, most of them calculate a scalar field from the velocity gradient and identify vortical structures by the iso-surface of these scalars when an arbitrarily threshold value is determined. The threshold somewhat represents the swirling strength of vortices, but the physical meanings of these scalars remain unclear. Furthermore, these methods more or less

* Projects supported by the National Key Research and Development Program of China (Grant Nos. 2019YFB1704200, 2019YFC0312400), the National Natural Science Foundation of China (Grant Nos. 51879159, 51909160).
Biography: Xin-wang Liu (1995-), Male, Ph. D. Candidate,
E-mail: huhgf670@163.com
Corresponding author: De-cheng Wan,
E-mail: dcwan@sjtu.edu.cn

involve shear and stretch contamination problems, where the shearing and stretching are both counted as a part of vortex strength. Finally, Liu et al.[6] creatively proposed the concept of Liutex, which is quite different from the first- and second-generation VI methods. The third-generation Liutex method is an eigenvalue-based method which is local, accurate, and unique[7]. Liutex is defined as a vector. One important feature of the Liutex system is its capability of providing the six core elements of vortex, namely, absolute strength, relative strength, local rotation axis, vortex rotation axis, vortex core size and vortex boundary, which can be regarded as touchstones to test vortex definition and visualization methods[8]. Here, the magnitude of Liutex represents the rotational strength of the fluid rotation, and the direction of Liutex represents the axis of local fluid rotation. Based on this, several methods including the Liutex magnitude iso-surface, objective Liutex [9], Liutex -Ω method[10-11], and Liutex core line method[12-13], which are classified as the third-generation VI methods, have been proposed and applied in recent years. Several commonly used vortex identification methods for marine hydrodynamics are revisited by Zhao et al.[14]

Based on the Liutex method, Yu and Wang[15] conducted a basic research of directly numerically manipulating vortices and obtain vortex dynamics and vortex control strategies. In their studies, two Liutex-based vortex control models, namely the centripetal force field model and the counter-rotation force field model, were proposed as a source term adding into the Navier-Stokes equations.

In this paper, the Liutex-based force field models and implementation of the centripetal force model are briefly introduced at first. The centripetal force field model is then applied to the slow-fat JBC ship sailing in calm water at the design speed Froude number 0.142 by altering the strength of the centripetal force source term. Finally, the results of parametric study on the strength of the centripetal force source term are further analyzed through the views including ship resistance and wake performances, and Liutex distributions.

1. Liutex vector and the centripetal force model implementation

First proposed by Liu et al.[6], the Liutex vector $\boldsymbol{R}$ is determined by rotating the velocity gradient tensor $\nabla\boldsymbol{u}$ to a special coordinate system where the rotation axis recombines with the local z-axis. When the other two eigenvalues of the velocity gradient tensor are complex conjugate[7], the rotation axis is the real eigenvector of the velocity gradient tensor. However, this definition is complex and difficult to numerically implement. To simplify the calculation, an explicit expression can be given by

$$\boldsymbol{R} = R\boldsymbol{r} = \left[\boldsymbol{\omega}\cdot\boldsymbol{r} - \sqrt{(\boldsymbol{\omega}\cdot\boldsymbol{r})^2 - 4\lambda_{ci}^2}\right]\boldsymbol{r} \tag{1}$$

where R represents the magnitude of $\boldsymbol{R}$, $\boldsymbol{r}$ is the real eigenvector of $\nabla\boldsymbol{u}$, $\boldsymbol{\omega}$ is the conventional vorticity vector, and λ_{ci} is the imaginary part of the complex eigenvalue of $\nabla\boldsymbol{u}$.

In order to directly control the vortices, the first consideration is to directly modify the Navier-Stokes equations by adding an additional source term to the right side of the momentum equation, which can be expressed by the following formula

$$\frac{\partial\boldsymbol{u}}{\partial t} + (\boldsymbol{u}\cdot\nabla)\boldsymbol{u} = -\nabla\frac{p}{\rho} + \nabla\cdot(\nu\nabla\boldsymbol{u}) + \boldsymbol{g} + c\boldsymbol{a} \tag{2}$$

Equation (2) controls the fluid motions for incompressible flow if the body force is caused by the gravity only, where $\boldsymbol{u}$, $\boldsymbol{g}$ are the velocity and the gravity acceleration vector, respectively, while p, ρ, ν represent the pressure, fluid density and kinematic viscosity, respectively, the c in the adding source term is a coefficient to control the strength of the Liutex force, and $\boldsymbol{a}$ is the Liutex-based force source term to be determined.

Two Liutex-based force field models were proposed in the previous work of Yu and Wang[15]. The first one is a centripetal force model, which is defined as

$$\boldsymbol{a} = \frac{\boldsymbol{R}}{2}\times\left(\frac{\boldsymbol{R}}{2}\times\boldsymbol{l}\right) = \frac{1}{4}\boldsymbol{R}\times(\boldsymbol{R}\times\boldsymbol{l}) \tag{3}$$

where $\boldsymbol{l}$ is a vector starting from any field point P and ending at the local minimum pressure point P_0, which serves as the central point of the vortex core. $\boldsymbol{R}/2$ is half of the Liutex vector and represents the angular velocity of the rigid rotation part at P around the center of the vortex core P_0.

The other force field model with a time scale τ is given by

$$\boldsymbol{a} = -\frac{1}{2\tau}\boldsymbol{R}\times\boldsymbol{l} \tag{4}$$

where the time scale acts like a relaxation time, during which the rigid rotation of the fluid gradually stops and as a result the velocity drops to zero.

Considering that the time scale τ is not easy to ensure a calm-water drag calculation since it is a steady state as a consequence, unlike the flow past a hydrofoil [8] or cylinder[16], in this paper, the centripetal force model is utilized as the Liutex-based force field model. The definition of length scale $\boldsymbol{l}$ in it is simplified to $\boldsymbol{l}=(\nabla \boldsymbol{u})^{-1}\boldsymbol{u}$ for general consideration[16].

The main purpose of this paper is to study the vortex dynamics by applying the Liutex-based force field model, and see if it can strengthen or weaken vortices in the flow field and alter the hydrodynamic performances of the ship sailing in calm water. Therefore, the solving procedures for the modified incompressible Navier-Stokes solver should be given at first: the Liutex vector $\boldsymbol{R}$ and corresponding source term vector $c\boldsymbol{a}$ is first calculated at current time step for each cell, and then the modified Navier-Stokes equations with additional source terms are solved to obtain the velocity and pressure field for the next time step, until the final solution time is reached.

2. Calm-water drag and wake performance evaluation of JBC ship

2.1 *Basic information of JBC hull*

The JBC (Japan Bulk Carrier) ship is designed by the National Maritime Research Institute (NMRI), Yokohama National University (YNU) and the Shipbuilding Research Center of Japan (SRAJ) as a Capesize bulk carrier, which has become an internationally recognized standard ship model, having abundant experimental results to be verified by numerical calculation. Its 3-D model is shown in Fig. 1, and detailed information of main particulars is shown in Table 1.

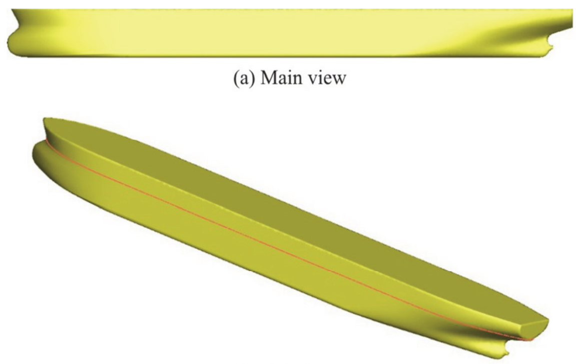

(a) Main view

(b) Global view

Fig. 1 (Color online) Geometry model of JBC

Table 1 Main particulars of JBC

Parameters	Symbol and unit	Value
Length between perpendiculars	L_{pp} /m	7
Breadth	B /m	1.125
Draught	T /m	0.4125
Molded depth	D /m	0.625
Drainage volume	∇ /m^3	2.786
Wet surface area	S_W /m^2	12.4

The JBC ship belongs to low-fat ship due to its low speed and big parallel middle body, making the viscous drag predominant. Furthermore, due to the large change of the curvature at the stern, the viscous pressure drag produces. In addition, the shape of the stern directly affects the velocity distribution at the propeller disk, which affects the wake performance.

In order to optimize its resistance and wake performance, the conventional practice is to carry out local deformations of the stern part of JBC ship (as shown in Fig. 2 using Free-Form Deformation method[17], where the red and green dots represent the moveable and fixed points, respectively). The hull form optimization aims to change the flow field by changing its boundary, and a series of researches on optimizing the shape of JBC ship hull or even wake equalizing duct has been done[18-19]. In addition, the Liutex force field model can also be considered to change the flow field, in order to reduce the pressure distribution at the stern of the ship and improve the axial wake field at the propeller disk, and the flow field is changed by applying additional source term to the flow field.

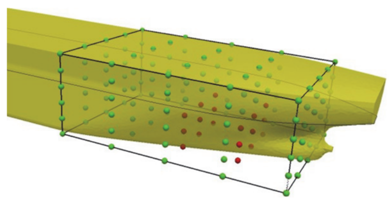

Fig. 2 (Color online) Stern deformation of JBC based on free-form deformation method

2.2 *Verification of numerical calculation of drag and flow field of JBC ship*

Firstly, the single-phase flow simulation of the JBC ship at model scale and design speed is carried out. The computational grid of single-phase flow does not consider the part above the calm water (the plane where the ship's design waterline is located). The size and boundary of the computational domain are shown in Fig. 3, and the specific boundary conditions are listed in Table 2. Grid refinement is mainly concentrated around the hull especially the bow and stern part, and the overall refinement condition is shown in Fig. 4. In addition, the numerical calculation results of two-phase flow will also serve as a reference and will be given below.

The vortice is expressed according to the Q-criterion. The calculated iso-surfaces (colored by axial velocity) of $Q=20$ near the hull by single-phase and two-phase flows are shown in Fig. 5. Seen from Fig. 5, the vortex distribution is almost the same at the underwater part of the hull, which reflects the similar viscous pressure resistance calculated by two methods.

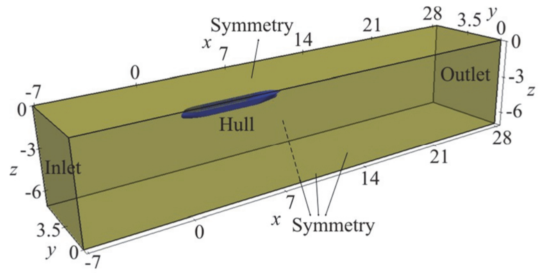

Fig. 3 (Color online) The size and boundaries of the computational domain for single-phase flow

Table 2 Summary of boundary conditions for single-phase flow

Boundary name	Condition
Inlet	Velocity inlet
Hull	No-slip wall
Symmetry	No-slip
Outlet	Pressure outlet

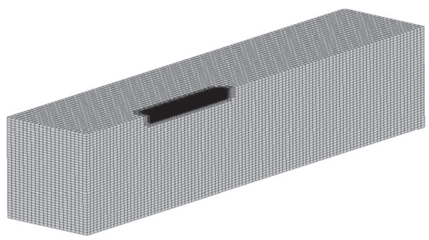

Fig. 4 The refinement settings of the computational domain for single-phase flow

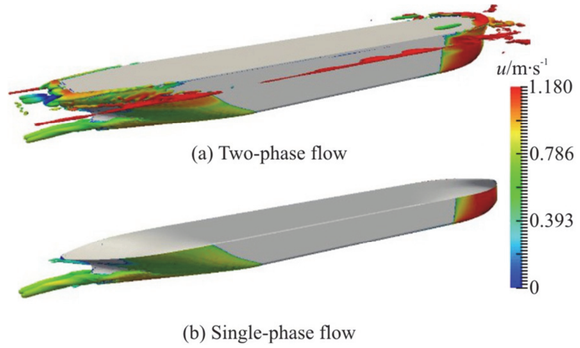

Fig. 5 (Color online) Comparison of Q calculated by two methods

Furthermore, the comparison of axial velocity distributions at the propeller disk is shown in Fig. 6. It is obvious that the wake field is almost the same, and the main difference is most likely due to the fact that the ship model releases the freedom of sinkage and trim during the calculation of two-phase flow, which leads to certain up and down deviation of the velocity distribution contour. In addition, the slight wave elevation on the free surface has little influence on the wake near the propeller shaft, indicating that using double-model method can evaluate the wake performance while making little difference with the result of viscous-based CFD method considering free surface.

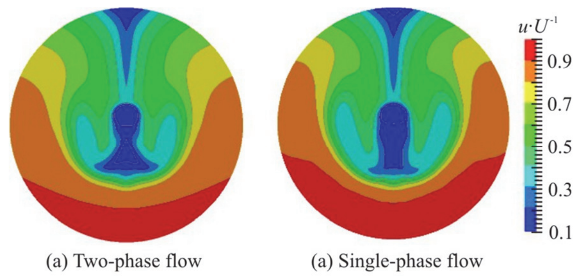

Fig. 6 (Color online) Comparisons of axial velocity distribution (u/U) near propeller disk

To sum up, in order to reduce the computational cost and speed up the convergence of the flow field after the source term is applied through the vortex field model, single-phase flow is considered in this paper to evaluate the total calm-water drag and the wake field at propeller disk of JBC ship.

According to the above setup of single-phase flow computational grid, the previously used single-phase flow computational grid is regarded as medium grid (S2), based on which a coarse grid (S3) and a fine grid (S1) can be generated respectively. The three sets of grids are shown in Fig. 7, and the size of the background grid of adjacent sets of grids is in a multifold relationship of $\sqrt{2}$ in each coordinate axis direction. The number of the three grids is shown in Table 3.

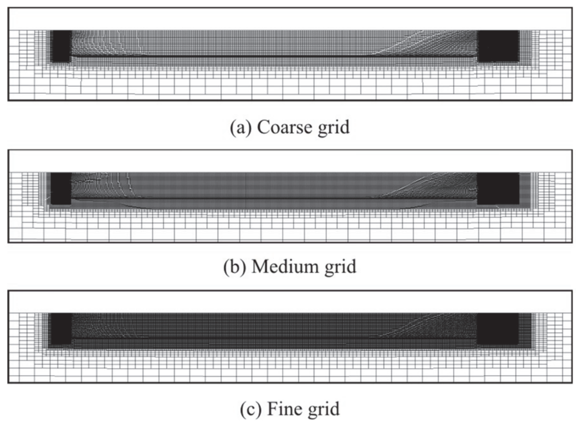

Fig. 7 Computational grids for grid uncertainty analysis

Table 3 Grid number settings of three sets

Grid No.	Background grid number	Total grid number
S3	70×14×28	878 722
S2	100×20×40	2 519 677
S1	140×28×56	6 747 658

The calculated results of the total drag and axial wake fraction under the three grids are shown in Table 4. As can be seen from Table 4, since the R_G values of the two physical quantities are all between 0 and 1 for the three sets of grids, the two physical quantities are monotonically convergent[20]. Theoretically, a convergent solution can be obtained by doing a series of refinement based on S2. Therefore, the grid layout is relatively reasonable, and the accuracy of using OpenFOAM to evaluate the resistance and wake performance can be verified. Finally, the subsequent numerical calculation adopt the medium grid (S2).

Table 4 Uncertainty analysis for JBC double-model calculation

Grid No.	Total drag, R_t /N	Wake fraction reduction $1-w$
S3	34.152	0.350
S2	32.702	0.347
S1	32.156	0.346
R_G	0.377	0.333

2.3 *Parametric study by using centripetal force model*

The centripetal force model is adopted to add the source term to the flow field. Due to the fact that the use of Liutex-based vortex field model to alter the control equations of the flow field can change the pressure and the vortices distributions of the flow field, in order to study the influence of different source term coefficients on the distribution of stern pressure and the wake at the propeller disk, 5 examples are designed in this paper. When the flow field is basically stable, the total drag and the fraction of axial wake at the propeller disk of the JBC ship are respectively calculated, and the results are listed in Table 5.

Table 5 Total drag and wake fraction reduction results for 5 cases

Case No.	c	Total drag, R_t /N	Wake fraction reduction $1-w$
Case 1	0	32.702	0.3471
Case 2	1	30.756	0.3467
Case 3	2	29.895	0.3436
Case 4	-1	39.189	0.3657
Case 5	-2	44.553	0.3723

It is not difficult to see from Table 5 that when the centripetal force is added to the Navier-Stokes equations as a source term, that is, $c>0$, the total drag and wake fraction reduction of JBC ship become smaller, and the greater the absolute value of c, the smaller the total drag and wake fraction reduction. On the contrary, when centripetal force is subtracted from the Navier-Stokes equations as a source term, that is, $c<0$, the total drag and the wake fraction reduction of JBC ship become larger, and the greater the absolute value of c, the larger the total drag and wake fraction reduction. To sum up, the total drag and wake fraction reduction both show a monotonous trend with respect to c, at least within a certain range of c. In particular, when $c=2$, the total drag drop reaches 8.58%, and the wake fraction reduction drop 1.01%, so the resistance and wake performances of JBC ship are both improved at this time. However, when $c=-2$, the total drag increases 36.23%, and the wake fraction reduction 7.26%, so the resistance and wake performances of JBC ship are both worse at this time. Therefore, it can be seen that the resistance and wake performances of JBC ship can be effectively improved when the centripetal force model is used to apply a source term with appropriate strength and $c>0$ into the Navier-Stokes equations.

It should be noted that the initial flow field of each case is the steady-state flow field when calculating the calm-water drag of the JBC ship under the single-phase flow with the simulation time 35 s, and the centripetal force source term is then added to the whole flow field at this moment. By monitoring the total drag of the JBC ship in the disturbed fields, as shown in Fig. 8, it can be found that about 2.4 s after the source term is applied, flow field of each case basically reaches a new stable state. In addition, it is not difficult to see that the greater the absolute value of c is, the greater the intensity of the source term acting on the flow field, that is, the greater the interference exerted on the original steady-state flow field, which will theoretically lead to a longer time for the flow field to reach the new stable state for the calm-water drag calculation.

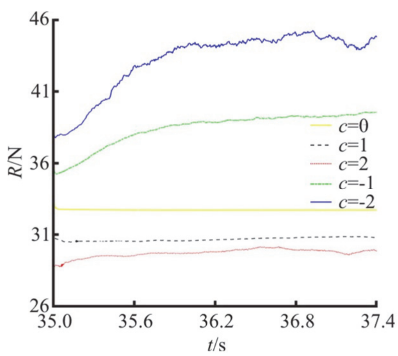

Fig. 8 (Color online) Comparison of time history of total drag for JBC ship in each case

Figure 9 shows the $\Omega_R=0.52$ iso-surface for case 1-5. Compared with case 1, due to the addition of the source term, the original steady flow field has disturbances, leading to the fluid rotation of the flow field even more active, especially in the region beyond a certain distance from the hull surface. Even so, for cases 2 and 3, the area of Ω_R iso-surface near the hull, especially near the stern of the ship, decreases to varying degrees, while for cases 4 and 5, the area of Ω_R iso-surface near the hull increases to some extent, which represents the changes of the viscous pressure drag of JBC ship. That is, in cases 2 and 3, the total drag of JBC ship decreases, while in cases 4 and 5, the total drag increases, which is consistent with the results in Table 5.

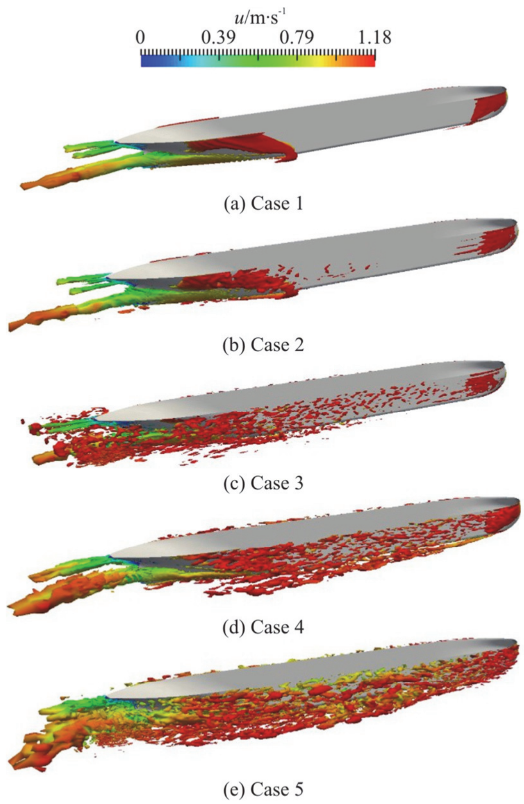

Fig. 9 (Color online) Comparison of Ω_R iso-surface of different cases

The comparison of the non-dimensional axial velocity distribution results at the propeller disk of JBC ship in case 2-5 is shown in Fig. 10. It can be seen that, compared with case 1, as shown in Fig. 6(b), since the fluid rotation in the flow field is more active due to the addition of the source term, the velocity distribution at the propeller disk will be directly affected. For cases 2 and 3, the high-speed area at the propeller disk somewhat increases, but the change is relatively small on the whole. For cases 4 and 5, the low-speed area near the propeller shaft increases significantly, which results in obvious compression of the high-speed area under the propeller shaft, and makes the wake fraction of JBC ship decrease more. In short, in cases 2 and 3, the wake fraction at the propeller disk of JBC ship is slightly increased, while in cases 4 and 5, the wake fraction at the propeller disk is relatively significantly decreased, which is consistent with the results in Table 5, that is, by adding the source term to the Navier-Stokes equations, the inflow of the propeller changes, which will alter the propulsion efficiency of the propeller and even the degree of cavitation.

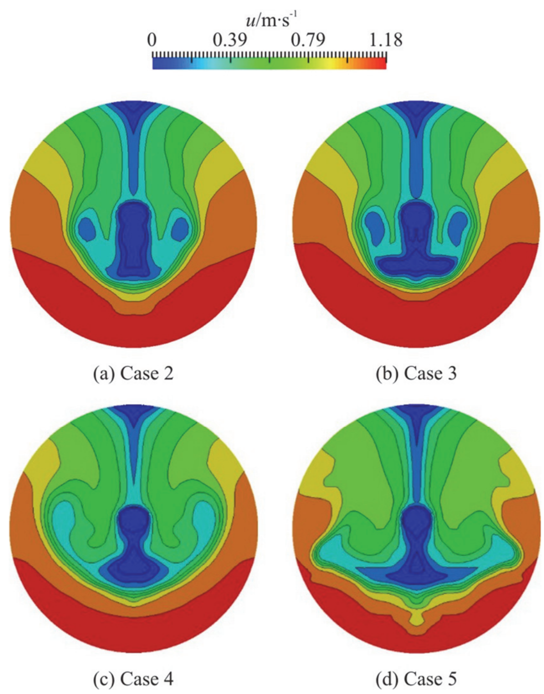

Fig. 10 (Color online) Comparison of axial velocity distribution at propeller disk of different cases

Figure 11 shows the comparison of the dynamic pressure distribution on the JBC hull surface of case 1-5. Obviously, compared with case 1, the pressure distribution of the flow field would change along with the velocity distribution due to the addition of the source term. For cases 2 and 3, the high-pressure and low-pressure regions on the hull surface change slightly on the whole. For cases 4 and 5, the high-pressure and low-pressure regions on the hull surface changes significantly, especially for case 5, which makes the total drag of JBC ship increase by 36.23% compared with case 1. In conclusion, the dynamic pressure distribution on the hull surface is consistent with the total drag results in Table 5, which further indicates that the resistance performance of the hull can be changed by applying the centripetal force model.

The following is to investigate the source term in the centripetal force model introduced in this paper, that is, the distribution of the amplitude of the source term $c\boldsymbol{a}$ induced by $\boldsymbol{R}$ around the JBC ship. Figure 12 shows the distribution comparison of $|c\boldsymbol{a}|$ around JBC in case 2-5. Case 1 is not given here, since $c = 0$ at this time. Compared with case 3, the $|c\boldsymbol{a}|$ of case 2 is smaller as a whole due to the smaller absolute value of c in case 2. Similarly, the $|c\boldsymbol{a}|$ of case 4 is smaller overall than that of case 5 because the absolute value of c in case 4 is smaller. In addition, although the absolute value of c in case 3 is the same as that in case 5, due to the different directions of the source term vector, the perturbation to the original steady flow field is completely different. Therefore, after further development (at the time of $t = 37$ s), distinct source term evolution forms are obtained.

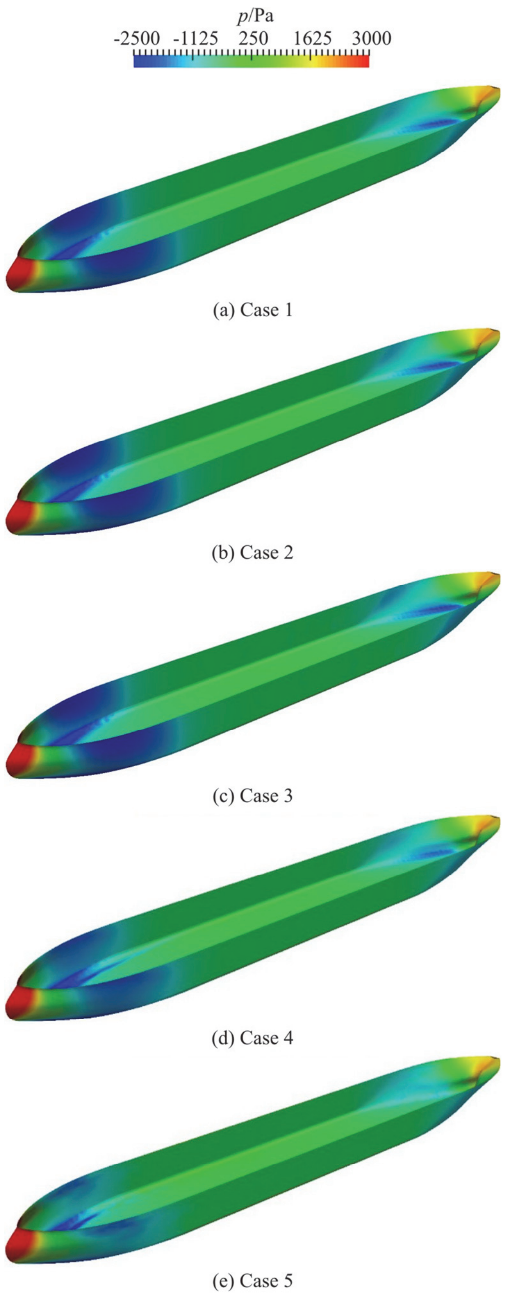

Fig. 11 (Color online) Comparison of pressure distribution on the hull surface of different cases

As a reference, the distribution of Liutex amplitude $|\boldsymbol{R}|$ around the JBC ship is finally given. Figure 13 shows the comparison of $|\boldsymbol{R}|$ distribution around JBC for cases 1, 3, and 5. Compared with case 1, the magnitude of Liutex under the stern plate of JBC is weakened to a certain extent in case 3, and the magnitude of Liutex behind the propeller shaft shows a "disrupt" form. However, larger Liutex is generated near the bottom of JBC in case 5. In addition, it should be noted that, in addition to the numerical correlation

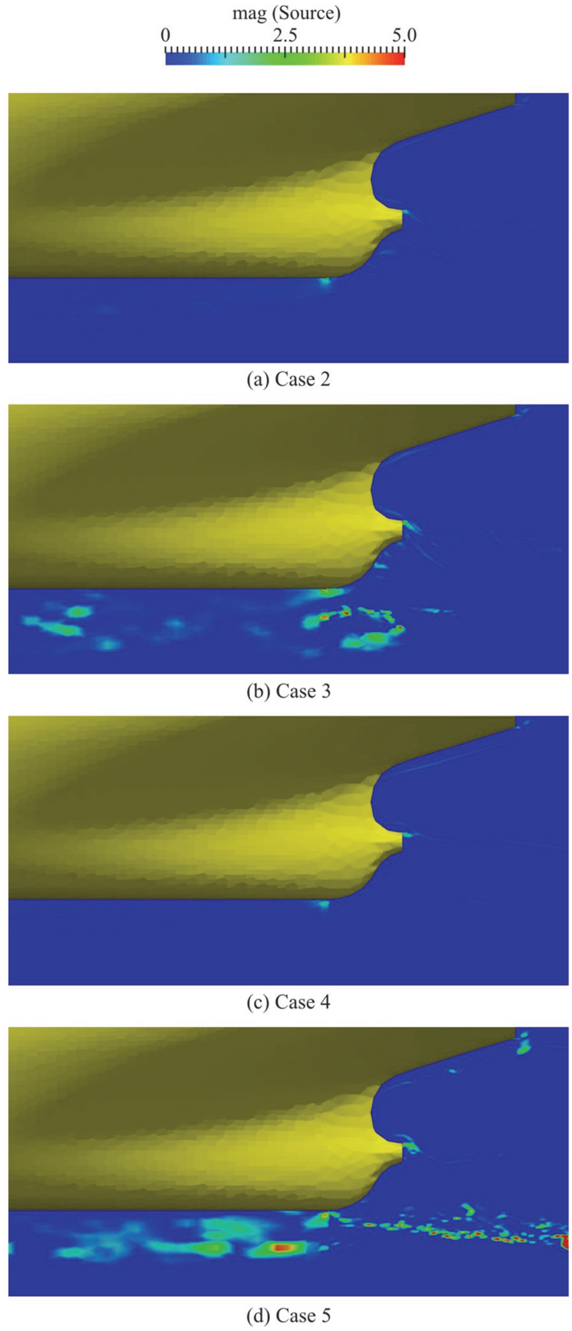

Fig. 12 (Color online) Comparison of magnitude of the source term distribution of different cases

between the amplitude of Liutex and the source term given by Eq. (3), combined with Fig. 12, it can be seen that the distribution of the two also has a strong spatial correlation, indicating that the centripetal force model based on Liutex can apply the source term according to the distribution of the Liutex, so the vortice distribution of the flow field can be effectively changed.

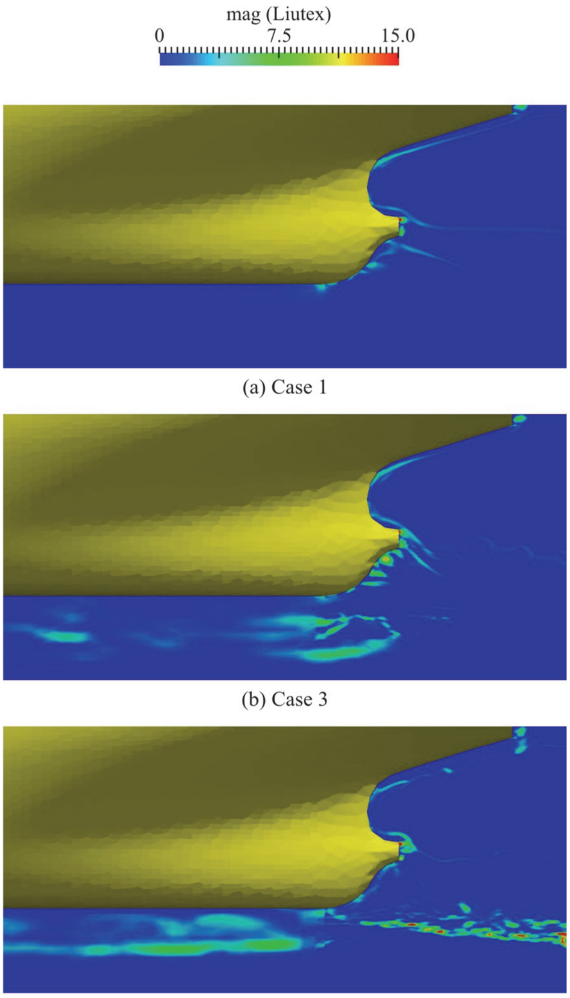

(a) Case 1

(b) Case 3

(c) Case 5

Fig. 13 (Color online) Comparison of magnitude of Liutex distribution of different cases

3. Conclusions

In this paper, the single-phase calm-water drag simulation of slow-fat JBC ship at its design speed is verified and the Liutex-based centripetal force model is applied to the steady-state flow around JBC ship, and the parametric study is done by altering the strength of the source term, that is, the coefficient c in order to investigate the influences of centripetal force on the flow field, and the resistance and wake performances of the JBC ship.

The total drag and wake fraction reduction of JBC both show a monotonous trend with respect to c, at least within a certain range of c. Particularly, when $c=2$, the total drag drop reaches 8.58%, and the wake fraction reduction drop 1.01%, so the resistance and wake performances of JBC ship are both improved at this time. Furthermore, the greater the absolute value of c is, the greater the strength of the source term acting on the flow field, which will theoretically lead to a longer time for the flow field to reach the new stable state for the calm-water drag calculation.

The Ω_R iso-surface, dynamic pressure distribution on the hull surface, as well as non-dimensional axial velocity distribution are all changed to some extent compared with the initial case (case 1), which demonstrate the change of the resistance and wake performances of JBC ship. Last but not least, the distribution of the amplitude of Liutex and the source term has a strong spatial correlation.

To sum up, apart from the change of the hull shape, the flow field can also be altered and controlled by adding the source term to strengthen or weaken the vortices, which gives us a new way to optimize the hydrodynamic performances of the marine structures. Therefore, future work will focus on adding rotating devices at the fore or stern part of the ship, which can equivalently substitute the numerical source term of the flow field, so as to change the vortices, and realize the optimization of comprehensive hydrodynamic performances of the ship by vortex-force-model based appendages design. Furthermore, the hull form deformation can be done at the regions where the amplitude of the source term according to the Liutex-based centripetal force model is relatively large. In this way can the vortex force field model guide the next-generation comprehensive hydrodynamic performances of the ship and even offshore structures.

References

[1] Liu C., Gao Y. S., Dong X. R. et al. Third generation of vortex identification methods: Omega and Liutex/Rortex based systems [J]. *Journal of Hydrodynamics*, 2019, 31(2): 205-223.

[2] Hunt J., Wray A., Moin P. Eddies, streams, and convergence zones in turbulent flows [R]. Proceedings of the Summer Program. Center for Turbulence Research Report CTR-S88, 1988, 193-208.

[3] Jeong J., Hussain F. On the identification of a vortex [J]. *Journal of Fluid Mechanics*, 1995, 285: 69-94.

[4] Chong M. S., Perry A. E., Cantwell B. J. A general classification of three-dimensional flow fields [J]. *Physics of Fluids A*: *Fluid Dynamics*, 1990, 2(5): 765-777.

[5] Zhou J., Adrian R. J., Balachandar S. et al. Mechanisms for generating coherent packets of hairpin vortices in channel

flow [J]. *Journal of Fluid Mechanics*, 1999, 387: 353-396.
[6] Liu C., Gao Y., Tian S. et al. Rortex–A new vortex vector definition and vorticity tensor and vector decompositions [J]. *Physics of Fluids*, 2018, 30(3): 035103.
[7] Gao Y., Liu C. Rortex and comparison with eigenvalue-based vortex identification criteria [J]. *Physics of Fluids*, 2018, 30(8): 085107.
[8] Wang Y. Q., Yu H. D., Zhao W. W. et al. Liutex-based vortex control with implications for cavitation suppression [J]. *Journal of Hydrodynamics*, 2021, 33(1): 74-85.
[9] Liu C. An objective version of the Rortex vector for vortex identification [J]. *Physics of Fluids*, 2019, 31(6): 065112.
[10] Dong X., Gao Y., Liu C. New normalized Rortex/vortex identification method [J]. *Physics of Fluids*, 2019, 31(1): 011701.
[11] Liu J. M., Liu C. Modified normalized Rortex/vortex identification method [J]. *Physics of Fluids*, 2019, 31(6): 061704.
[12] Liu C., Gao Y. S., Liu J. M. et al. A Liutex based definition of vortex rotation axis line [J]. *Journal of Hydrodynamics*, 2019, 31(3): 445-454.
[13] Xu H., Cai X. S., Liu C. Liutex (vortex) core definition and automatic identification for turbulence vortex structures [J]. *Journal of Hydrodynamics*, 2019, 31(5): 857-863.
[14] Zhao W. W., Wang J. H., Wan D. C. Vortex identification methods in marine hydrodynamics [J]. *Journal of Hydrodynamics*, 2020, 32(2): 286-295.
[15] Yu H. D., Wang Y. Q. Liutex-based vortex dynamics: A preliminary study [J]. *Journal of Hydrodynamics*, 2020, 32(6): 1217-1220.
[16] Zhao W. W., Wang Y. Q., Chen S. T. et al. Parametric study of Liutex-based force field models [J]. *Journal of Hydrodynamics*, 2021, 33(1): 86-92.
[17] Liu X., Wang J., Wan D. Hull form optimization design of KCS at full speed range based on resistance performance in calm water [C]. *Proceedings of the 28th International Ocean and Polar Engineering Conference*, Sapporo, Japan, 2018, 626-632.
[18] He P., Filip G., Martins J. et al. Design optimization for self-propulsion of a bulk carrier hull using a discrete adjoint method [J]. *Computers and Fluids*, 2019, 192: 104259.
[19] Furcas F., Vernengo G., Villa D. et al. Design of wake equalizing ducts using RANSE-based SBDO [J]. *Applied Ocean Research*, 2020, 97: 102087.
[20] Stern F., Wilson R. V., Coleman H. W. et al. Comprehensive approach to verification and validation of CFD simulations–Part 1: Methodology and Procedures [J]. *Journal of Fluids Engineering*, 2001, 123(4): 793-802.